
**Liquid Crystals**
Publication details, including instructions for authors and subscription information:
http://www.informaworld.com/smpp/title~content=t713926090

# Studies of nematic-isotropic transition for a Gay-Berne fluid using the second virial approximation

Valeriy V. Ginzburg[a]; Matthew A. Glaser[a]; Noel A. Clark[a]
[a] Condensed Matter Laboratory, Department of Physics, University of Colorado, Boulder, CO, U.S.A.

**To cite this Article** Ginzburg, Valeriy V. , Glaser, Matthew A. and Clark, Noel A.(1996) 'Studies of nematic-isotropic transition for a Gay-Berne fluid using the second virial approximation', Liquid Crystals, 21: 2, 265 — 271
**To link to this Article: DOI:** 10.1080/02678299608032832
**URL:** http://dx.doi.org/10.1080/02678299608032832

LIQUID CRYSTALS, 1996, VOL. 21, NO. 2, 265–271

# Studies of nematic–isotropic transition for a Gay–Berne fluid using the second virial approximation

by VALERIY V. GINZBURG*, MATTHEW A. GLASER and NOEL A. CLARK

Condensed Matter Laboratory, Department of Physics, University of Colorado, Boulder, CO 80309-0390, U.S.A.

(*Received 20 December 1995; accepted 19 March 1996*)

In this paper we use the second virial approximation to study the nematic–isotropic (N–I) transition for a Gay–Berne liquid for a broad range of parameters. For Gay–Berne hard Gaussian overlap (HGO) fluid particles we found that a N–I transition exists as a function of density for all length to breadth ratios $\kappa > 4$, in reasonable agreement with other theoretical studies and results of Monte Carlo simulations. For the full Gay–Berne potential (GB) the location of the N–I transition as a function of density for different temperatures was studied for several values of shape and energy anisotropy parameters $\kappa$ and $\kappa'$. It was shown that the transition temperature increases or the transition density decreases with increasing $\kappa$ and/or decreasing $\kappa'$. Wherever the molecular dynamics (MD) or Monte Carlo (MC) data were available, comparison was made. For each system, coexistence density and pressure were calculated, and, wherever possible, also compared with MC or MD data to show qualitative agreement. The reported study is considered to be a first step in the calculation of N–I transition for rigid liquid crystal (LC) molecules.



## 1. Introduction

In recent years, significant progress has been achieved in the modelling of orientational ordering in liquid crystals. Of particular interest was the role of different types of intermolecular interactions in the formation of ordered phases. Both the long-range attractive and short-range repulsive forces are important in the process of orientational ordering, and theories of nematic ordering based on either type of interaction have existed for a long time. After the pioneering work of Maier and Saupe [1] (theoretical description of nematic–isotropic transition due to attractive orienting intermolecular potential) and of Onsager [2] (theoretical model of athermal nematic–isotropic transition due to steric excluded-volume effects), many successful attempts were made to simulate these systems and verify predictions of both theories. The role of attractive potential has been investigated, e.g. in a Lebwohl–Lasher lattice model [3]. Athermal excluded-volume interactions were studied in several simulations of hard body molecules (ellipsoids of revolution, spherocylinders) by Frenkel and co-workers [4, 5]. It was shown that steric interactions may result in not only nematic ordering, but sometimes in formation (at higher densities) of smectic or crystal phases. In particular, hard spherocylinders can form isotropic, nematic, smectic A and crystal phases, while, e.g. elongated hard ellipsoids of revolution have isotropic, nematic and crystal phases (no smectics). However, the question of relative importance of these two types of interaction (steric hard-core repulsion and orienting attraction) was unresolved and required a simple model correctly including both features.

Such analysis became possible after Berne *et al.* [6] introduced an orientation-dependent analogue of the standard Lennard–Jones (LJ) intermolecular potential. Like LJ, the Gay–Berne potential includes both long-range attractive and short-range repulsive parts; however, its parameters strongly depend upon the relative orientation of interacting molecules. The Gay–Berne (GB) potential has the same symmetry as ellipsoids of revolution; thus, the difference between the phase behaviour of the GB-system and that of hard ellipsoids has to be ascribed to the attractive part of the potential. That is why the GB model is now widely used to model phase behaviour of liquid crystals.

In their study of the GB system using Monte Carlo and NVT (constant particle number, volume and temperature) molecular dynamics, de Miguel *et al.* [7, 8] found several mesophases, including isotropic, nematic, smectic (or hexatic) B, tilted smectic B. Luckhurst *et al.* [9] analysed a slightly modified GB potential using the same method to find isotropic, nematic, smectic A and crystal phases. The system of GB hard ellipsoids (precise defini-

*Author for correspondence.

0267–8292/96 $12·00 

tion of this will be given later in the text) and truncated GB potential with only a repulsive part were also studied using the same MD technique. De Miguel *et al.* found [8] that such systems do not exhibit any smectic phases, in agreement with the symmetry argument due to Frenkel that such smectic phases would be impossible, since hard ellipsoids can be transformed to hard spheres by affine compression.

Some theoretical attempts were made recently to calculate the GB phase diagram using a density functional approach and perturbation methods. Velasco *et al.* [10] applied a perturbation scheme with the hard Gaussian overlap (HGO) model as a reference, to calculate phase coexistence in a full GB system. The improvement in determining the N–I transition densities and coexistence region, however, was not very significant in comparison with the Onsager mean-field approximation.

In spite of all the success of numerical studies of the GB system, there has been, to our knowledge, no systematic attempt to study the influence of the shape and energy anisotropy on the N–I transition temperatures and pressures. Although the GB potential allows one uniquely to explore this dependence, the full investigation of the phase diagram in the complete parameter space using any of the aforementioned methods would require very large computational effort. On the other hand, it should be interesting and important to visualize qualitative dependence of transition parameters on the interaction anisotropies, since it could be applied to understand, for example, dependence of transition temperature on molecular length in homologous series.

In order to analyse such qualitative trends and dependencies, we employ the second virial (also known as Onsager) approximation. While this approximation oversimplifies intermolecular correlations and is known to break down at low temperatures and/or high densities, it is very easy to carry out and very computationally inexpensive. By applying it to a set of GB fluids with different shape and energy anisotropies, it is possible to obtain the N–I transition temperature (at a given pressure) or coexistence pressure and densities (at a given temperature) as functions of both anisotropies. Comparison of the results obtained with the known data from MC and MD simulations would then suggest ways of systematically improving the theory.

In this paper we report the calculated phase diagram of the Gay–Berne system using the second virial approximation. We calculate coexistence pressures and densities for a number of parameters to analyse how the change in either shape or energy anisotropy affects the phase diagram. Whenever possible, we compare the phase diagrams obtained with MC or MD results.

Our paper is organized as follows. In § 2, we describe the second virial approximation and introduce distribution functions, order parameters and thermodynamic variables. § 3 contains the description of the GB potential as used in our calculations, and other specific details of the calculation. In § 4, results of the calculation are summarized and phase diagrams for several values of GB potential parameters are shown. Finally, § 5 contains brief conclusions and suggestions for future applications.

## 2. Second virial approximation

Let us assume that particles in the fluid are cylindrically symmetric (they could have ellipsoidal, spherocylindrical or cylindrical shape), i.e. belong to $D_{\infty h}$ symmetry group and can freely rotate about the long axis. In this case, orientation of a given molecule is determined by its two Euler angles, the polar angle $\theta$ and the azimuthal angle $\varphi$.

We introduce the single-particle distribution function $\gamma(\Omega)$ (note that $\gamma$ is a function of $\theta$ only and does not depend on $\varphi$ for symmetry reasons) and the pair correlation function $g(1,2) = g(\theta_1, \varphi_1, \theta_2, \varphi_2, \mathbf{r}_{12})$, where $\mathbf{r}_{12}$ is a vector connecting centres of molecules 1 and 2. In the second virial approximation, the Helmholtz free energy of a spatially uniform phase (nematic or isotropic) is given by:

$$F = \rho V k_B T \int d\Omega \gamma(\Omega) \ln [4\pi\gamma(\Omega)] + \frac{1}{2}\rho^2 V k_B T \int\int\int d\Omega_1\, d\Omega_2\, d^3\mathbf{r}_{12} \gamma(\Omega_1)\gamma(\Omega_2) g(1,2) \times \ln \{g(1,2) \exp [\beta \Phi(1,2)]\}, \quad (1)$$

where $\Omega = (\theta, \varphi)$, $\rho$ is the number density, $V$ is the volume, $T$ is the temperature, $k_B$ is Boltzmann's constant, $\beta = (1/k_B T)$, and $\Phi(1,2) = \Phi(\Omega_1, \Omega_2, \mathbf{r}_{12})$.

Minimization of equation (1) with respect to $g$ and $\gamma$ subject to the constraint $\int d\Omega \gamma(\Omega) = 1$, yields the following self-consistency equations:

$$g(1,2) = \exp [-\beta \Phi(1,2)], \quad (2a)$$

$$\ln \gamma(\Omega_1) = C + \rho \int\int d\Omega_2\, d^3\mathbf{r}_{12} \gamma(\Omega_2)[g(1,2) - 1], \quad (2b)$$

$$\int d\Omega \gamma(\Omega) = 1, \quad (2c)$$

where $C$ is a normalization constant whose value is determined from equation (2 *c*).

In order to simplify the calculation, we seek the solution of equations (2 *a–c*) among the functions of a specific form:

$$\gamma(\Omega) = A \exp [\alpha Y_{20}(\theta, \varphi)], \quad (3)$$

where $A$ and $\alpha$ are parameters characterizing the degree of ordering, and $Y_{20}$ is a second spherical harmonic

function defined as:

$$Y_{20}(\theta,\varphi)=\left(\frac{5}{4\pi}\right)^{1/2}\left(\frac{3\cos^2\theta-1}{2}\right). \tag{4}$$

The functional form (3) stems from the spherical harmonic expansion of $\ln(\gamma)$ and the requirement that $\gamma$ is independent of $\varphi$ and even in $\cos\theta$. In this case, we can truncate the expansion after the first non-constant term to obtain (3). Our calculations showed that including the second and third terms in the expansion does not significantly change the results, so the simplest form (3) was used.

After substituting (3) into (2), we obtain equations for $A$ and $\alpha$ that should be solved iteratively. It is easy to show that the isotropic phase ($\alpha=0$, $A=1/4\pi$) is always a solution; at high enough densities and/or low enough temperatures, another solution with non-zero $\alpha$ (nematic) may exist and correspond to a state with lower pressure and free energy. The second virial approximation allows us to calculate the coexistence pressure, coexistence densities, and the jump of the nematic order parameter at the transition, for each temperature.

The nematic order parameter $S$ and pressure $P$ are given by:

$$S=\int \mathrm{d}\Omega\gamma(\Omega)\left(\frac{3\cos^2\theta-1}{2}\right), \tag{5}$$

$$P=k_{\mathrm{B}}T\rho-\frac{1}{2}k_{\mathrm{B}}T\rho^2\int\int\int \mathrm{d}\Omega_1\,\mathrm{d}\Omega_2\,\mathrm{d}^3\mathbf{r}_{12}\times\gamma(\Omega_1)\gamma(\Omega_2)f(1,2), \tag{6}$$

where $f(1,2)=\exp[-\beta\Phi(1,2)]-1$ is the Mayer function.

## 3. Intermolecular potential and details of calculation

As we noted in §1, the GB potential is one of the most widely used for description of phase behaviour of thermotropic liquid crystals due to its relative simplicity and ability to vary the relative strengths of steric repulsion and anisotropic attraction. The most common form for the GB potential is:

$$U_{\mathrm{GB}}=4\varepsilon(\mathbf{r},\mathbf{u}_1,\mathbf{u}_2)\left\{\left[\frac{\sigma_0}{r-\sigma(\mathbf{r},\mathbf{u}_1,\mathbf{u}_2)+\sigma_0}\right]^{12}-\left[\frac{\sigma_0}{r-\sigma(\mathbf{r},\mathbf{u}_1,\mathbf{u}_2)+\sigma_0}\right]^{6}\right\} \tag{7}$$

where $r=|\mathbf{r}_1-\mathbf{r}_2|$, $\mathbf{r}=(\mathbf{r}_1-\mathbf{r}_2)/r$ is a unit vector along the line connecting the centres of masses of molecules 1 and 2, $\mathbf{u}_i$ is a unit vector along the symmetry axis of the $i$th molecule; $\sigma(\mathbf{r},\mathbf{u}_1,\mathbf{u}_2)$ and $\varepsilon(\mathbf{r},\mathbf{u}_1,\mathbf{u}_2)$ are orientation-dependent Lennard–Jones parameters, given by:

$$\sigma(\mathbf{r},\mathbf{u}_1,\mathbf{u}_2)=\sigma_0\left\{1-\frac{\chi}{2}\left[\frac{(\mathbf{r}\cdot(\mathbf{u}_1+\mathbf{u}_2))^2}{1+\chi\mathbf{u}_1\cdot\mathbf{u}_2}+\frac{(\mathbf{r}\cdot(\mathbf{u}_1-\mathbf{u}_2))^2}{1-\chi\mathbf{u}_1\cdot\mathbf{u}_2}\right]\right\}^{-1/2}, \tag{8}$$

$$\varepsilon(\mathbf{r},\mathbf{u}_1,\mathbf{u}_2)=\varepsilon_0[1-\chi^2(\mathbf{u}_1\cdot\mathbf{u}_2)^2]^{-m/2}\times\left\{1-\frac{\chi'}{2}\left[\frac{(\mathbf{r}\cdot(\mathbf{u}_1+\mathbf{u}_2))^2}{1+\chi'\mathbf{u}_1\cdot\mathbf{u}_2}+\frac{(\mathbf{r}\cdot(\mathbf{u}_1-\mathbf{u}_2))^2}{1-\chi'\mathbf{u}_1\cdot\mathbf{u}_2}\right]\right\}^{n}, \tag{9}$$

$\chi=(\kappa-1)/(\kappa+1)$, $\chi'=(\kappa'^{1/2}-1)/(\kappa'^{1/2}+1)$, where $\kappa$ is the length-to-breadth ratio (shape anisotropy), and $\kappa'$ is the ratio of the potential well depths for the side-by-side and end-to-end configurations (energy anisotropy).

Exponents $m$ and $n$ are: $m=1$, $n=2$ in the original Gay–Berne work [6] and in the simulations of de Miguel *et al.* [7, 8], and $m=2$, $n=1$ in the simulations of Luckhurst *et al.* [9]. (According to Luckhurst, this modification of potential makes side-by-side configuration relatively more advantageous in comparison with some intermediate positions and thus stimulates smectic ordering). In our work, original exponents $m=1$, $n=2$ were used, although trial calculations were performed with Luckhurst's exponents to find out that there were no qualitative differences between phase diagrams for these cases.

We also analysed the Gay–Berne HGO fluid (or Gay–Berne hard ellipsoids), in which:

$$\begin{aligned} U&=\infty, \quad r<\sigma(\mathbf{r},\mathbf{u}_1,\mathbf{u}_2),\\ U&=0, \quad r\geqslant\sigma(\mathbf{r},\mathbf{u}_1,\mathbf{u}_2),\end{aligned} \tag{10}$$

where $\sigma(\mathbf{r},\mathbf{u}_1,\mathbf{u}_2)$ is given by (8). The properties of this system should be similar to those of hard ellipsoids, although some differences could lead to the difference in phase behaviour for relatively small length-to-breadth ratios.

For the case of the Gay–Berne potential, phase diagrams were calculated for length-to-breadth ratios $\kappa=3, 3{\cdot}25, 3{\cdot}5, 3{\cdot}75, 4, 4{\cdot}5, 5, 5{\cdot}5, 6$, and for energy anisotropies $\kappa'=5, 10, 20, 40$; for HGO hard particles, the same length-to-breadth ratios were studied. For the case of Gay–Berne, a cut-off radius $R_{\mathrm{C}}=6\sigma_0$ was used.

Integration of the right-hand side of equations (2*b*) and (6) is performed using the repeated trapezoidal rule. Due to the cylindrical symmetry, the number of variables over which integration is done, is reduced by one. We used the following number of mesh-points: 4 for $\varphi$ (azimuthal angle), 8 for $\theta$ (polar angle), 20 for $r_\perp$

(perpendicular component of **r**) and 24 for $r_{\parallel}$ (parallel component of **r**).

When solving equations (2*b*,*c*) with parametrization (3), an iterative procedure was used, with convergence criterion $|\alpha_n - \alpha_{n-1}| < 0{\cdot}01$.

For each temperature in the case of regular GB, or at temperature 1·0 in the case of HGO hard particles, calculation is done for 25 densities between 0·01 and 0·5 with a step of 0·02 (all densities are measured in units of $\sigma_0^{-3}$, and all temperatures are measured in units of $\varepsilon_0$).

## 4. Results and discussion

### 4.1. *HGO hard particles*

For HGO hard particles, an N–I transition was found for length-to-breadth ratios larger than 3·75. For $\kappa \leqslant 3{\cdot}75$, no transition was observed, indicating that there is no stable nematic phase in this region. This result agrees approximately with Monte Carlo data for hard spherocylinders (where the N–I transition is observed for $\kappa > 4$) and hard ellipsoids, where $\kappa$ should be larger than 3 for transition to take place (see, e.g. [11]). In figure 1, a phase diagram for HGO hard particles is shown, with coexistence densities determined using the Maxwell rule. It is difficult to compare exactly the HGO model with either of the two other hard particle models (spherocylinders or hard ellipsoids) since parameter $\kappa$ (shape anisotropy) has a different definition in each model. However, it is possible to state qualitatively that, as expected from the second virial model, the calculated coexistence regions are significantly broader than the simulated ones. In figure 2, the coexistence pressure is plotted as a function of the length-to-breadth ratio. It can be seen that coexistence pressure decreases with increasing $\kappa$, as expected.

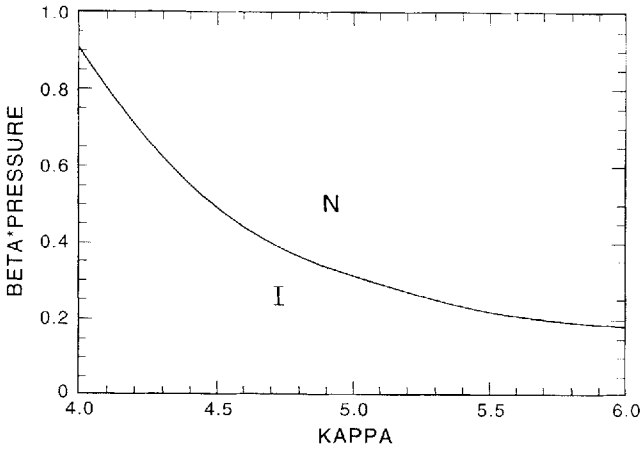


Figure 2. Transition pressure $\beta P$, where $\beta = 1/k_B T$, as a function of shape anisotropy $\kappa$ for HGO system. N denotes nematic phase, I isotropic phase.

### 4.2. *GB fluid*

For the GB system, the attractive part of the potential makes orientational ordering easier than in HGO. It is though hard to judge *a priori* whether the energy anisotropy helps or hinders the orientational ordering, so one of the first priorities was to see how the transition temperatures and/or densities depend on $\kappa'$ for the fixed $\kappa$. In figure 3, the coexistence densities are shown for the GB system with $\kappa = 3$, at temperature $T = 2{\cdot}0$, for several values of $\kappa'$. It is seen clearly that increase in energy anisotropy hinders, rather than helps, orientational ordering, albeit very slightly. In figure 4, coexistence pressures are shown for the same set of parameters. Again, a small but noticeable increase in coexistence pressure can be seen with increasing energy anisotropy. In figure 5, we analyse the dependence of transition

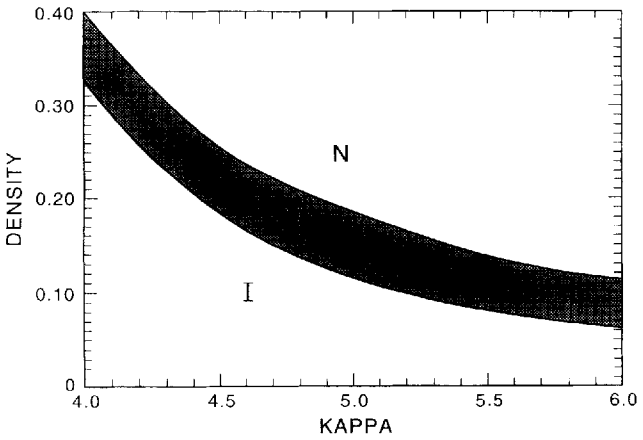


Figure 1. Coexistence densities of the HGO system in the second virial approximation as functions of shape anisotropy $\kappa$. N denotes nematic phase, I isotropic phase; the coexistence region is shaded.

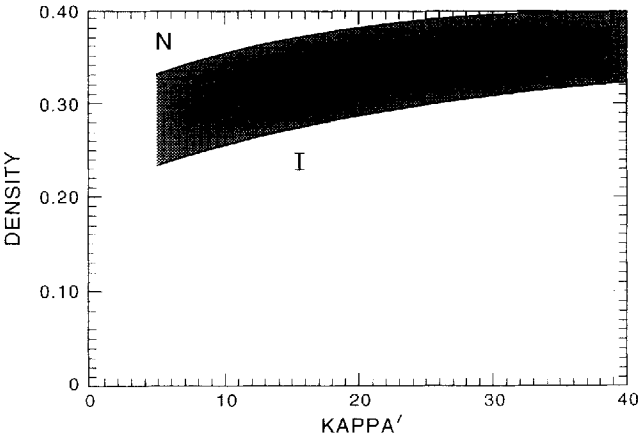


Figure 3. Coexistence densities of the GB system as functions of energy anisotropy $\kappa'$ in the second virial approximation. Shape anisotropy $\kappa = 3$. N denotes nematic phase, I isotropic phase; the coexistence region is shaded.

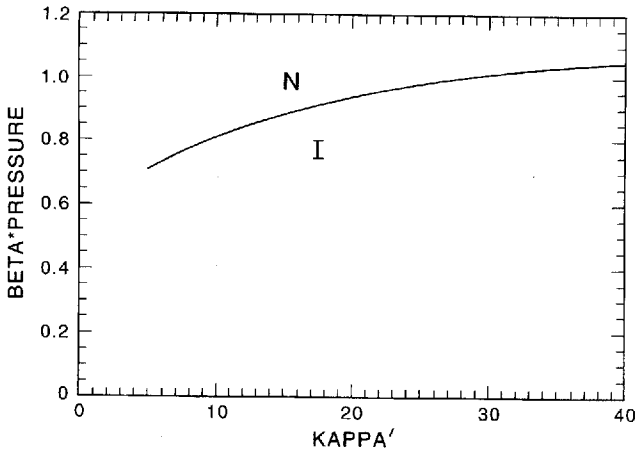


Figure 4. Transition pressure $\beta P$, where $\beta = 1/k_B T$, as a function of energy anisotropy $\kappa'$ in the second virial approximation. Shape anisotropy $\kappa = 3$. N denotes nematic phase, I isotropic phase.

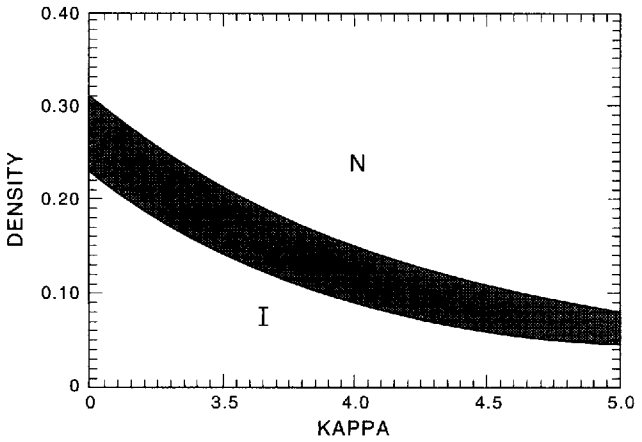


Figure 5. Coexistence densities of the GB system as functions of shape anisotropy $\kappa$ in the second virial approximation. Energy anisotropy $\kappa' = 5$. N denotes nematic phase, I isotropic phase; the coexistence region is shaded.

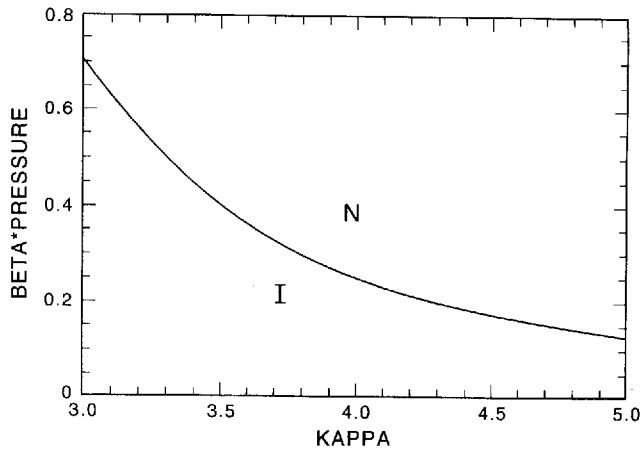


Figure 6. Transition pressure $\beta P$, where $\beta = 1/k_B T$, as a function of shape anisotropy $\kappa$ in the second virial approximation. Energy anisotropy $\kappa' = 5$. N denotes nematic phase, I isotropic phase.

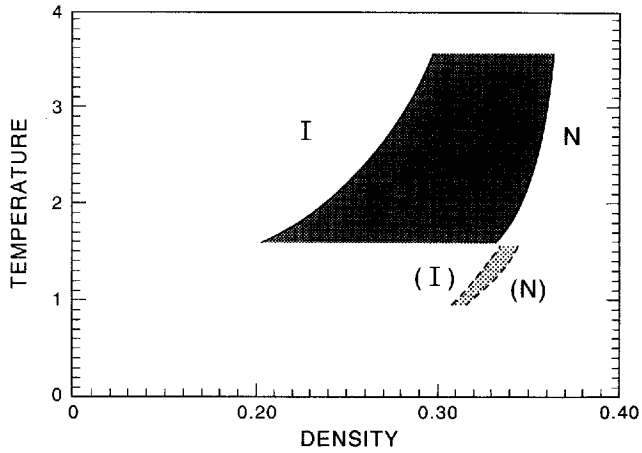


Figure 7. Phase diagram for the GB system with $\kappa = 3$, $\kappa' = 5$. Solid lines are for the coexistence densities in the second virial approximation, dashed lines are the Monte Carlo results from [8]. N, (N), I, (I) denote nematic and isotropic phases, respectively, in the SVA and in the MC.

density on shape anisotropy. At $T = 2{\cdot}0$, $\kappa' = 5$, coexistence densities are shown for several different values of $\kappa$. As in the case of hard particles, coexistence densities drop when shape anisotropy increases. In figure 6, coexistence pressures are plotted for the same set of parameters, showing a decrease in coexistence pressure with an increasing shape aniostropy.

In order to compare the results produced by the second virial approximation with the results of Monte Carlo or molecular dynamics studies, we analysed in detail the behaviour of the system with $\kappa = 3$, $\kappa' = 5$. The temperature dependence of N–I transition for this system is shown in figure 7, compared with that calculated by de Miguel *et al.* [7, 8] (our calculation results—solid lines, de Miguel's results—dashed lines). It can be seen again that the second virial approximation produces a significantly broader coexistence region; it also predicts that the nematic phase becomes stable at $T = 1{\cdot}4$, while the MC result for this value is 0·8. However, the results of the second virial approximation have to be treated with caution at low temperatures, because it does not take into account other ordered phases (smectics and crystals).

In figure 8, the coexistence pressure $\beta P$ is plotted as a function of temperature, compared with the MC simulations of de Miguel *et al.* It can be seen that second virial approximation underestimates transition pressure for this system very strongly; this can be ascribed to the fact that in the second virial theories, effects of steric repulsion, significant at high densities, are not correctly

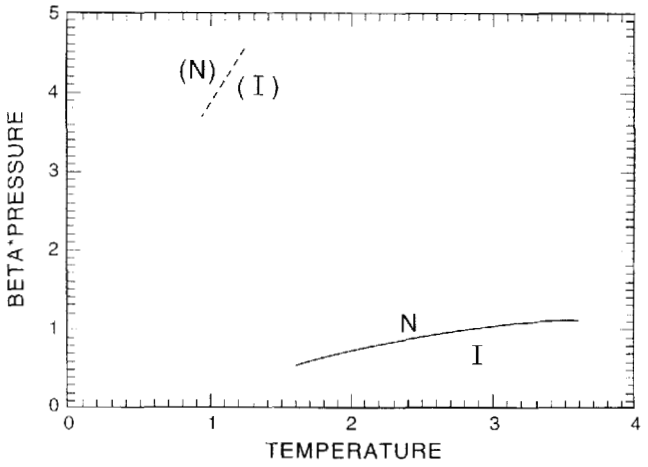


Figure 8. Transition pressure $\beta P$, where $\beta = 1/k_B T$, as a function of temperature, for the system $\kappa = 3$, $\kappa' = 5$. The solid line corresponds to the pressures calculated using the second virial approximation; the dashed line represents the Monte Carlo data from [8]. N, (N), I, (I) denote nematic and isotropic phases, respectively, in the SVA and in the MC.

accounted for. One would expect that the discrepancy should be smaller if a transition is to occur at smaller densities, but it is difficult to verify due to the lack of computational data for other parts of the parameter space.

In order to summarize the calculation results for different shape and energy anisotropies, in figure 9 the three-dimensional surface plots of transition pressures at temperatures (*a*) 1·6, (*b*) 2·0, and (*c*) 2·4 are shown for different values of $\kappa$ and $\kappa'$. This graphically illustrates the trends already discussed, i.e. that coexistence pressures and densities increase with the increase in shape anisotropy and decrease with the increase in energy anisotropy. In figure 10, three-dimensional plots of transition temperatures are made for a fixed coexistence pressure of 1·0.

The surface plots of figures 9 and 10 represent different cross-sections of the full phase diagram for a regular Gay–Berne potential. At present only very few points on this phase diagram have been studied using MC or MD: the already mentioned work by de Miguel *et al.* [7, 8] for $\kappa = 3$, $\kappa' = 5$, and the study of a point $\kappa = 4{\cdot}4$, $\kappa' = 40$ by Luckhurst and Simmonds [12] (the direct comparison with the latter work is difficult because simulations were performed at a fixed density of 0·16, rather than at fixed pressure, and because the different exponents $\mu = 0{\cdot}8$ and $\nu = 0{\cdot}74$ were used). It can be seen that attractive interaction obviously decreases the nematic–isotropic transition temperature for a fixed density or pressure, and, in some instances, allows the formation of a nematic phase in a region where the

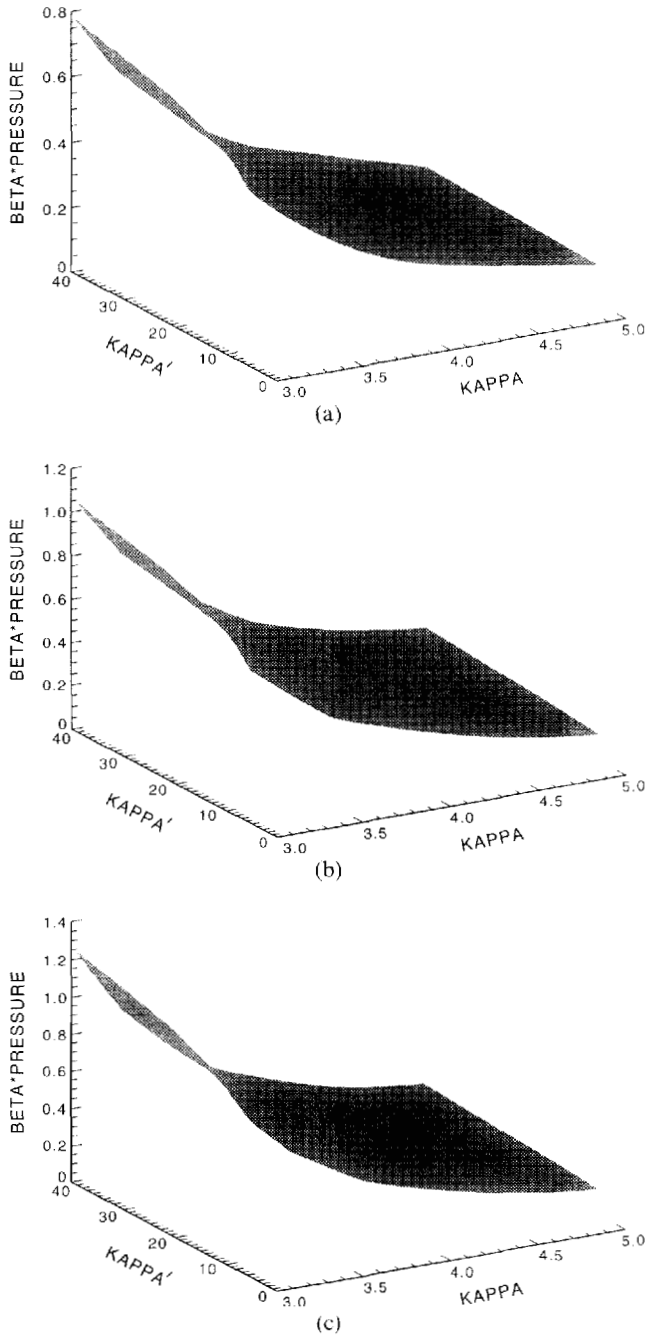


Figure 9. Three-dimensional plot of transition pressure $\beta P$, where $\beta = 1/k_B T$, as a function of $\kappa$ and $\kappa'$ for (*a*) $T = 1{\cdot}6$ (*b*) $T = 2{\cdot}0$, and (*c*) $T = 2{\cdot}4$.

HGO system does not exhibit any transition at all (e.g. $\kappa = 3$).

## 5. Conclusions

We calculated the phase behaviour of GB HGO and GB particles over a broad range of shape and energy anisotropies using the second virial (Onsager) approxi-

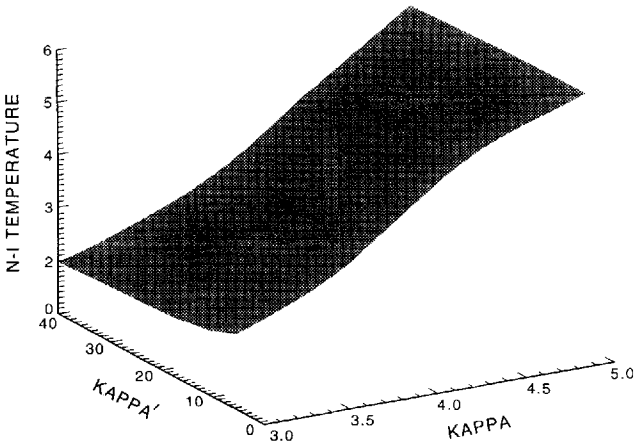


Figure 10. Three-dimensional plot of transition temperature $T_{NI}$ as a function of $\kappa$ and $\kappa'$ at pressure $P = 1{\cdot}0$.

mation. Coexistence temperatures and pressures for the nematic–isotropic transition were calculated at a large number of points in Gay–Berne parameter space, enabling us to visualize the dependencies of these characteristics on various anisotropies of the potential. The obtained results, as always with second virial-type calculations, could be expected to yield significant errors for high densities and/or low temperatures. Unfortunately, absence of reliable Monte Carlo or molecular dynamic results for most regions in the Gay–Berne parameter space do not allow one to estimate these errors (with the exception of the point $\kappa = 3$, $\kappa' = 5$).

It is shown that in the Gay–Berne model, the increase in shape anisotropy and/or the decrease in energy anisotropy increases the N–I transition temperature at fixed density or pressure. While the first part of this conclusion is well-known (longer rods align at lower densities even without attractive interaction), the second part is not that obvious and depends on the specifics of the potential and the way energy anisotropy is varied. Since the energy parameter $\varepsilon_0$ is kept constant, the depth of the 'side-by-side' potential well remains the same, but depths of the 'end-to-end' and all the intermediate wells decrease with the increase in energy anisotropy and vice versa. This effect makes the nematic phase less favourable for the large $\kappa'$. Moreover, since the increase in energy anisotropy favours the 'side-by-side' ordering, one could argue that at some large enough $\kappa'$ the nematic phase would shrink completely, leading to a direct isotropic–smectic A transition.

The calculated phase diagram does not take into account the possible formation of smectic or crystal phases. It is possible, therefore, that in some cases, the nematic phase obtained could turn out to be metastable, and a direct isotropic–smectic A, isotropic–hexatic B, or isotropic–crystal transition would take place instead. In view of the previous discussion, it is highly likely to expect such a phase diagram for systems with high energy anisotropies. However, the lack of computational data again makes the discussion of these possibilities difficult.

The improvement upon the second virial approximation could be achieved using either integral equation (e.g. Percus–Yevick or hypernetted chain approximations) or density functional methods. Even though in recent years, these methods were applied with a varying degree of success to isotropic and nematic phases of GB fluid, the understanding of more ordered phases is not yet achieved.

Apart from academic interest, calculation of phase diagrams for Gay–Berne potential could have a practical significance in the light of recent attempts to parametrize intermolecular potentials for relatively rigid liquid crystalline mesogens using a regular or biaxial Gay–Berne potential [12, 13]. If this approach proves to be useful, experimental data for the observed nematic–isotropic transition temperatures could be used to analyse the calculated GB phase diagram and vice versa.

This work was supported by the National Science Foundation under Materials research Grant DMR 92-02312. We thank D. Walba and E. Garcia for useful discussions.

## References

[1] (*a*) MAIER, W., and SAUPE, A., 1958, *Z. Naturforsch. A*, **13,** 564; (*b*) 1959, *ibid*, **14,** 882; (*c*) 1960, *ibid*, **15,** 287.
[2] ONSAGER, L., 1949, *Ann. N. Y. Acad. Sci.*, **51,** 62.
[3] (*a*) LEBWOHL, P. A., and LASHER, G., 1972, *Phys. Rev. A*, **6,** 426; (*b*) 1973, *ibid*, **7,** 2222.
[4] (*a*) EPPENGA, R., and FRENKEL, D., 1984, *Mol. Phys.*, **52,** 1303; (*b*) FRENKEL, D., MULDER, B. M., and MCTAGUE, J. P., 1984, *Phys. Rev. Lett.*, **52,** 287.
[5] (*a*) FRENKEL, D., and MULDER, B. M., 1985, *Mol. Phys.*, **55,** 1171; (*b*) FRENKEL, D., 1987, *ibid*, **60,** 1, (*c*) 1988, *J. phys. Chem.*, **92,** 3280.
[6] (*a*) BERNE, B. J., and PECHUKAS, P., 1972, *J. chem. Phys.*, **56,** 4213; (*b*) GAY, J. G., and BERNE, B. J., 1981, *ibid*, **74,** 3316.
[7] DE MIGUEL, E., RULL, L. F., CHALAM, M. K., GUBBINS, K. E., and VAN SWOL, F., 1991, *Mol. Phys.*, **72,** 593.
[8] DE MIGUEL, E., RULL, L. F., CHALAM, M. K., and GUBBINS, K. E., 1991, *Mol. Phys.*, **74,** 405.
[9] LUCKHURST, G. R., STEPHENS, R. A., and PHIPPEN, R. W., 1990, *Liq. Cryst.*, **8,** 451.
[10] VELASCO, E., SOMOZA, A. M., and MEDEROS, L., 1995, *J. chem. Phys.*, **102,** 8107.
[11] ALLEN, M. P., EVANS, G. T., FRENKEL, D., and MULDER, B. M., 1993, *Adv. Chem. Phys.*, **LXXXVI,** 1.
[12] LUCKHURST, G. R., and SIMMONDS, P. S. J., 1993, *Mol. Phys.*, **80,** 233.
[13] BERARDI, R., FAVA, C., and ZANNONI, C., *Chem. phys. Lett.*, 1995, **236,** 462.